

Discovery of Spiro-azaindoline Inhibitors of Hematopoietic Progenitor Kinase 1 (HPK1)

Bryan K. Chan,* Eileen Seward, Michael Lainchbury, Thomas F. Brewer, Le An, Toby Blench, Matthew W. Cartwright, Grace Ka Yan Chan, Edna F. Choo, Jason Drummond, Richard L. Elliott, Emanuela Gancia, Lewis Gazzard, Baihua Hu, Graham E. Jones, Xifeng Luo, Andrew Madin, Sushant Malhotra, John G. Moffat, Jodie Pang, Laurent Salphati, Christopher J. Sneeringer, Craig E. Stivala, Binqing Wei, Weiru Wang, Ping Wu, and Timothy P. Heffron



Cite This: *ACS Med. Chem. Lett.* 2022, 13, 84–91



Read Online

ACCESS |



Metrics & More



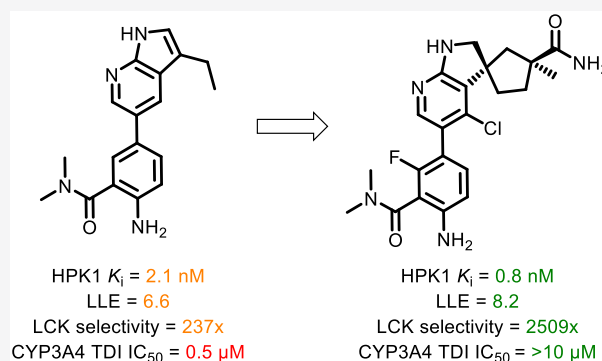
Article Recommendations



Supporting Information

ABSTRACT: Hematopoietic progenitor kinase 1 (HPK1) is implicated as a negative regulator of T-cell receptor-induced T-cell activation. Studies using HPK1 kinase-dead knock-in animals have demonstrated the loss of HPK1 kinase activity resulted in an increase in T-cell function and tumor growth inhibition in glioma models. Herein, we describe the discovery of a series of small molecule inhibitors of HPK1. Using a structure-based drug design approach, the kinase selectivity of the molecules was significantly improved by inducing and stabilizing an unusual P-loop folded binding mode. The metabolic liabilities of the initial 7-azaindole high-throughput screening hit were mitigated by addressing a key metabolic soft spot along with physicochemical property-based optimization. The resulting spiro-azaindoline HPK1 inhibitors demonstrated improved *in vitro* ADME properties and the ability to induce cytokine production in primary human T-cells.

KEYWORDS: HPK1, immuno-oncology, structure-based design, kinase inhibitor, CYP inhibition



In contrast to traditional anticancer therapies where the goal is to target pathways that drive tumor proliferation or survival, cancer immunotherapies aim to leverage the patient's own immune system to combat tumors.¹ Over the past several years, a number of antibody inhibitors of immune checkpoints have found considerable clinical success by enhancing cancer patients' immune T-cell activity. The survival benefits engendered by those approved antibody inhibitors have been impressive; however, the response rate to these agents remains modest. Hence, there is tremendous interest in the identification of additional agents to complement the approved immunomodulators.²

Hematopoietic progenitor kinase 1 (HPK1) is a member of the Ste20 serine/threonine family of kinases that serves as a negative regulator of T-cell receptor (TCR) induced T-cell activation.³ Studies using HPK1 kinase-dead knock-in mouse models have demonstrated that HPK1 kinase activity limits TCR signaling and cytokine production.⁴ In preclinical syngeneic models, loss of HPK1 kinase function was found to suppress tumor growth. Given the compelling evidence, HPK1 has been proposed to be a promising cancer immunotherapy target.⁵ As such, the goal of our program was to identify a selective small molecule inhibitor of HPK1.

A high-throughput screen using the kinase domain of HPK1 yielded compound **1**, a literature Abl inhibitor⁶ (Abl IC_{50} < 0.51 nM), as a promising hit with respect to potency for HPK1 (K_i = 0.4 nM) and lipophilic ligand efficiency⁷ (LLE = 6.3). In addition to activity against Abl, **1** also showed inhibitory activity against LCK (IC_{50} = 24 nM, 55-fold selectivity over HPK1). Since Abl⁸ and LCK⁹ are essential components of cell survival and TCR signaling, respectively, improving selectivity against these two off-targets was a major focus of our optimization effort.

To improve selectivity against Abl, we first explored the difference in the ATP binding site gatekeeper residue between HPK1 (Met) and Abl (Thr).¹⁰ Due to the shorter Thr side chain in Abl, modeling suggested that Abl would suffer from a greater loss of favorable van der Waals interactions if the size of the C3 substituent of the azaindole motif were reduced (R_1 in Table 1). Gratifyingly, conversion of the anisole substituent (**1**, Abl IC_{50} <

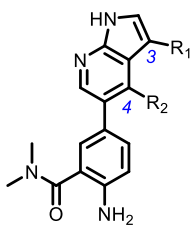
Received: August 30, 2021

Accepted: December 1, 2021

Published: December 8, 2021



Table 1. Optimization of 7-Azaindoles



compd	R ₁	R ₂	cLogP	HPK1 K _i (nM) ^a	LLE ^b	Abl selectivity ^c	LCK selectivity ^d
1	2-MeOPh	H	3.1	0.4	6.3	<1×	55×
2	Et	H	2.1	2.1	6.6	10×	237×
3	H	H	1.5	130	5.4		66×
4	Et	Me	2.4	0.4	7.0	58×	808×
5	Et	Et	2.8	0.2	6.9		2556×
6	Et	Cl	2.6	0.5	6.7		501×

^aAll apparent K_i values represent arithmetic means of at least two determinations using the HPK1 Lantha binding biochemical assay. ^bLLE, lipophilic ligand efficiency based on HPK1 K_i. ^cSelectivity expressed as the ratio of Abl K_i over HPK1 K_i. ^dSelectivity expressed as the ratio of LCK K_i over HPK1 K_i.

0.51 nM) to the smaller ethyl group (2, Abl IC₅₀ = 22 nM) resulted in considerable improvement in selectivity against Abl while improving the LLE against HPK1. The increase in LLE suggested that the small alkyl substituent was better suited for HPK1 binding. While compound 2 exhibited only modest Abl selectivity, this promising result suggested that optimizing other vectors of the ligand using a structure-based approach may further enhance the selectivity against Abl.

An X-ray structure of 3 bound to HPK1 revealed a binding mode that was atypical among kinase structures (Figure 1A). While the 7-azaindole motif engaged the hinge region of the kinase in a canonical manner, the P-loop of the kinase adopted an unusual “folded” conformation. In the “folded P-loop” conformation, the side chain of Tyr28 was positioned to engage the ligand through hydrophobic interactions.¹¹ Furthermore, the main-chain peptide bond N–H of Gly24 in the P-loop is directed toward the ligand and engaged the amide carbonyl of the ligand via a hydrogen bond.

In contrast, in the more usual “extended P-loop” conformation (as exemplified by G1858;¹² Figure 1B), both structural features (Gly24 N–H and Tyr28 side chain) would not be available to interact with the azaindole ligands. In the “extended” conformation, the N–H of Gly24 forms a hydrogen bond with Val31 within the P-loop β-sheet, while the side chain of Tyr28 is situated in the DFG region of the binding pocket, away from the hinge region.¹²

The “folded” P-loop conformation is not commonly observed among kinases that have been studied.¹¹ The ability of HPK1 to adopt the folded conformation was attributed to the unusually high number of glycine residues within its P-loop resulting in a high degree of flexibility, a feature that is absent in the LCK sequence. Literature examples suggested that stabilizing or engaging the “folded” P-loop conformation may have the potential to improve selectivity.^{11,13} Hence, we hypothesized that further engagement of Gly24 and Tyr28 in the folded P-loop conformation of HPK1 may result in improvement in both potency and selectivity against our key off-target LCK and the wider kinome.

To further optimize the interactions between the 7-azaindole ligands and Tyr28 in the folded P-loop, small lipophilic substituents at the C4 position (R₂ in Table 1) were evaluated. Compared to the parent molecule 2 (R₂ = H), installation of a

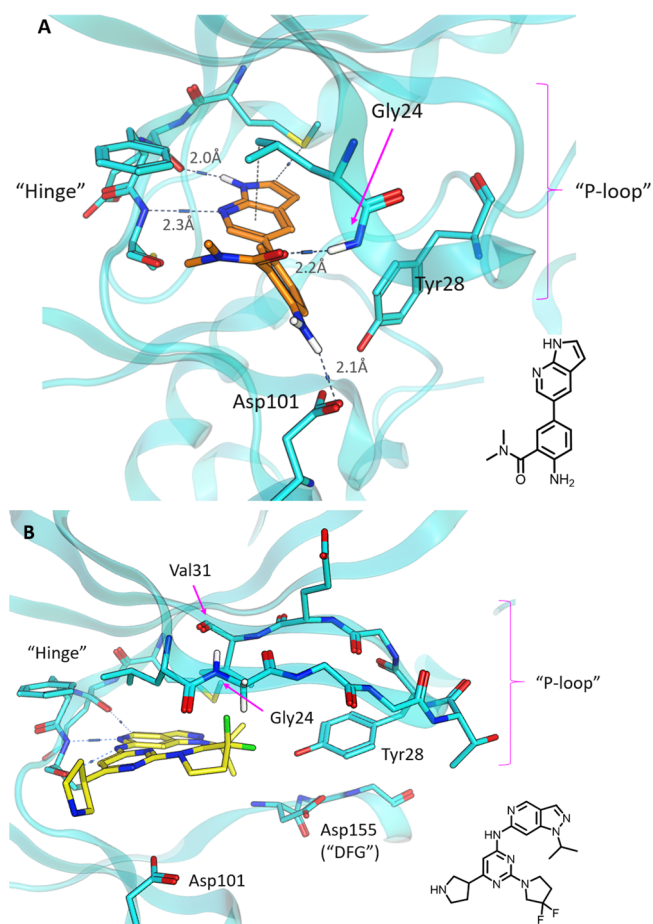


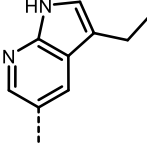
Figure 1. (A) X-ray structure of 3 bound in HPK1 (PDB: 7R9L) and (B) X-ray structure of G1858¹² bound in HPK1 (PDB: 7R9N). Predicted hydrogen bond interactions are shown as dashed lines. Distances from N/O to hydrogen are shown.

methyl (4), ethyl (5), or chloro (6) group afforded gains in potency for HPK1 and improved selectivity against LCK and Abl (compound 4). It is also noteworthy that the alkyl substitutions at C4 also improved the LLE of the molecules, suggesting that productive interactions were established. Encouraged by the potency and selectivity of the 3-ethyl-7-

azaindole series, our attention turned to improvement of the ADME-PK properties.

As shown in Table 2, compound 2 showed high turnover in human liver microsomes and time-dependent inhibitory activity

Table 2. Optimization of Solvent-Exposed Region



Cmpd	Structure	HPK1 K_i (nM) ^a	LCK Selectivity ^b	LM H/R/M ^c	CYP 3A4 TDI IC ₅₀ (μM) ^d
2		2.1	237x	12/25/80	0.5
7		5.2	157x	18/43/84	1.7
8		3.3	735x	17/28/81	1.6
9		0.47	1958x	16/37/80	0.7

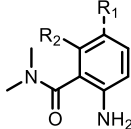
^aAll apparent K_i values represent arithmetic means of at least two determinations using the HPK1 Lantha binding biochemical assay. ^bSelectivity expressed as the ratio of LCK K_i over HPK1 K_i . ^cLM = Liver microsomes clearance measured in mL/min/kg, H = human, R = rat, M = mouse. ^dCYP3A4 time-dependent inhibition (TDI) assay performed using testosterone as a probe substrate.

against CYP3A4. Attempts to attenuate oxidative metabolism, such as deletion of the amino group (7) or installation of an electron-withdrawing group (8 and 9), did not improve *in vitro* metabolic stability (as measured by lowering of human liver microsomal clearance) or address time-dependent inhibition of CYP3A4. Interestingly, introduction of a fluoro substituent improved both the potency for HPK1 and selectivity against LCK. Based on modeling, we hypothesized that the fluorine atom occupies a lipophilic pocket and stabilizes the nonplanar conformation of the ligand such that its aniline N–H could effectively hydrogen-bond with Asp101 (see Figure 1A). It is also worthy to note that, compared to analogues with primary or secondary amides, analogues with a tertiary amide (such as 2) demonstrated superior potency and selectivity against LCK (data not shown). We hypothesized that the tertiary amide preferred to reside in an out-of-plane conformation relative to the aniline such that the carbonyl group was well-positioned to hydrogen bond with the backbone N–H of Gly24. Given the lack of impact on metabolism with modifications within the aniline portion of the molecule, the focus of our optimization efforts then shifted to the 7-azaindole motif.

Despite the presence of the 7-aza substitution, the electron-rich 5-membered ring within the 7-azaindole motif was implicated as the primary cause of oxidative metabolism and time-dependent inhibitory activity against CYP3A4.¹⁴ Examination of the X-ray cocrystal structure of 3 bound to HPK1 suggested that further substitutions at the 2- and 3-positions of

the 7-azaindole should be tolerated and could provide opportunities to address the metabolic issues. Installation of a chlorine atom (10) at the 2-position to sterically and inductively deactivate the azaindole toward oxidation failed to improve human liver microsome (HLM) stability and time-dependent inhibition of CYP3A4 (Table 3).

Table 3. Optimization of Hinge-Binding Azaindole Group



Cmpd	R1	R2	cLogP	HPK1 K_i (nM) ^a	LLE ^b	LCK Selectivity ^c	HLM ^d	CYP 3A4 TDI IC ₅₀ (μM) ^e
2	H	H	2.1	2.1	6.6	237x	12	0.50
9	F	H	2.1	0.5	7.2	1665x	15	0.70
10	H	Cl	2.5	2.7	6.1	>9000x	14	0.20
11	H	Cyclopropyl	0.95	33	6.5	176x	8	>10
12	H	Cyclobutyl	1.4	66	5.8	89x	10	>10
13	H	Cyclopentyl	1.8	28	5.8	166x	7	9.8
14	F	Cyclopropyl	1.5	43	5.9	>9000x	9	6.5
15	F	Cyclobutyl	2.1	2.2	6.6	1340x	16	>10
16	F	Cyclopentyl	2.5	6.7	5.7	325x	17	0.8

^aAll apparent K_i values represent arithmetic means of at least two determinations using the HPK1 Lantha binding biochemical assay. ^bLLE, lipophilic ligand efficiency based on HPK1 K_i . ^cSelectivity expressed as the ratio of LCK K_i over HPK1 K_i . ^dHLM = Human liver microsomes predicted clearance (mL/min/kg). ^eCYP3A4 time-dependent inhibition (TDI) assay performed using testosterone as a probe substrate.

Further modeling suggested saturation of the azaindole to the corresponding azaindoline system should be tolerated and would also provide alternate exit vectors for structure-based design. 3-Spiro-cyclopropyl-indoline 11 demonstrated encouraging potency against HPK1 while reducing human liver microsome turnover and CYP inhibition. Expansion of the spiro-cyclopropyl ring to the cyclobutyl (12) or cyclopentyl groups (13) were also well-tolerated and offered alternative design exit vectors. In general, the spiro-indoline analogues showed a promising combination of good metabolic stability (as measured by HLM), minimal time-dependent inhibition of

CYP3A4, acceptable potency, and selectivity that warranted further optimization.

As predicted by the SAR from the 7-azaindole series, installation of a small lipophilic group at the 4-position of the spiro-azaindoline (14–16) to enhance the van der Waals interactions with Tyr28 led to improved selectivity against LCK (14–16) and potency for HPK1 (15, 16). However, possibly due to the increase in lipophilicity, the C4 substitution resulted in the erosion of metabolic stability and undesired CYP3A4 inhibition. This observation suggested that a reduction in general lipophilicity would be required to maintain a balance between potency and metabolic stability.

An X-ray structure of 14 bound to HPK1 (Figure 2) revealed a binding mode that was similar to that of the 7-azaindole HPK1

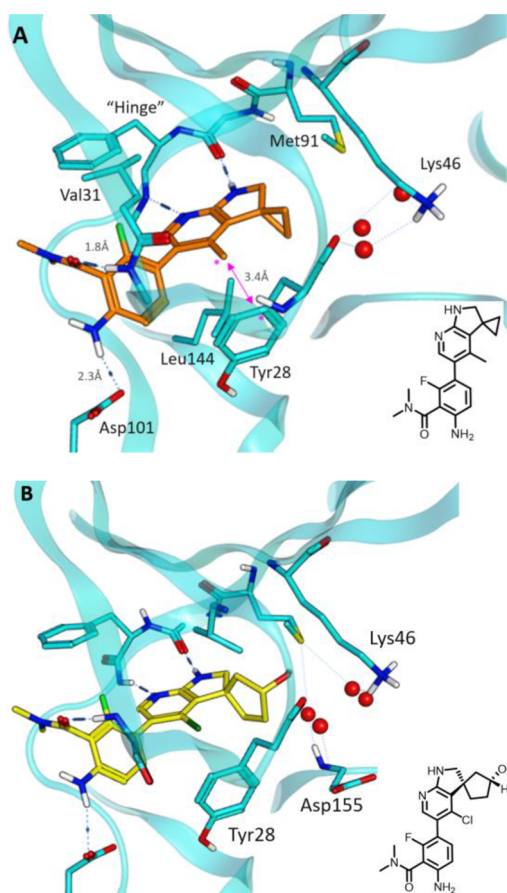


Figure 2. X-ray structures of (A) 14 (PDB: 7R9P) and (B) 17 (PDB: 7R9T) bound to HPK1. Red circles represent water molecules. Predicted hydrogen bonds: Interactions are shown as dashed lines; distances from N/O to hydrogen are shown. Pink arrow represents the distance between the carbons labeled with asterisks.

inhibitors, where the indoline motif formed two hydrogen bonding interactions with the hinge residues of HPK1. The carboxyl-aniline group extended toward solvent where the aniline N–H formed a hydrogen bonding interaction with Asp101. The phenolic side chain of Tyr28 engaged the inhibitor via hydrophobic interactions. The spirocyclic cyclopropyl ring occupied a pocket flanked by the Met90 gatekeeper residue, Leu144, Val31, and a water network in the direction of the catalytic Lys46. A close examination of this region of the binding pocket suggested that installation of polar groups on the spirocyclic system should not only reduce the overall lip-

ophilicity of the molecules, but also engage polar functionalities in the vicinity of Lys46.

While the cyclobutyl analogue 15 was superior with respect to LLE, modeling suggested that the larger cyclopentyl (16) or cyclohexyl templates should provide vectors and distances that are more suited to target Lys46. To test this hypothesis, a series of alcohol- and nitrile-functionalized analogues of 16 were designed to indirectly interact with Lys46 via the water network. Hydroxylated analogues 17–19 demonstrated HPK1 activity comparable to the parent 16 while improving *in vitro* metabolic stability significantly (Table 4). The nitrile analogues 20 and 21 maintained potency without improving HLM stability. An X-ray structure of 17 bound to HPK1 (Figure 2B) showed that the binding pose was identical to that of 14 with the hydroxyl group forming several hydrogen bonding interactions with the water network adjacent to Lys46. This observation was consistent with the increase in LLE and suggested that productive interactions were formed between the polar functionalities and the binding site.

To further improve HPK1 potency, we opted to design extended substituents that may directly engage Lys46 or its neighboring polar functionalities. Introduction of a primary amide (22) resulted in a gain in LLE, which suggested productive hydrogen bonding interactions were made. While demonstrating good HLM stability (HLM = 7.4 mL/min/kg), 22 only showed modest permeability (MDCK apical-to-basolateral $P_{app} = 0.2 \times 10^{-6} \text{ cm s}^{-1}$), possibly due to the high number of hydrogen bond donors (five) and high topological polar surface area (114 Å²). We anticipated that this might limit oral bioavailability; thus, we turned our attention to improving the permeability of 22.

Our strategy to improve permeability involved (a) reducing the number of hydrogen bond donors and (b) sterically masking the polar functionalities. Conversion of the primary amide to a secondary amide (compound 23) failed to maintain potency. Installing a methyl group adjacent to the amide (24) maintained potency and metabolic stability but did not improve permeability. Replacing the amide with other bioisosteres such as a triazole (27) resulted in loss of potency. Interestingly, expansion to the cyclic lactams (28 and 29) improved permeability while maintaining potency. When compared to 23 (where the *N*-methyl-amide likely existed preferentially in the *s-trans* conformation), the amide moiety in 28 and 29 was restricted to the *s-cis* conformation that may have maintained productive H-bonding interactions with the protein. We hypothesized that the increase in lipophilicity and steric shielding of the polar amide drove the improvement in permeability. However, the increase in lipophilicity also eroded metabolic stability.

Despite its low permeability as measured by the MDCK assay, we were encouraged by the potency and metabolic stability in HLMs of 24. Hence, its single enantiomers were isolated to give compounds 25 and 26. The two single enantiomers were tested in a cellular assay that measures the direct phosphorylation of SLP76 by HPK1 in Jurkat cells. Gratifyingly, compound 25 showed strong inhibitory effects in the cellular assay despite its modest MDCK permeability. Compound 25 also showed excellent selectivity against key off-targets such as LCK as well as in a broader kinase panel (5/47 kinases inhibited >70% at 0.1 μM; Abl inhibited at <35% at 0.1 μM). To evaluate its stimulatory effect on immune response, human pan T-cells were treated with 25 for 4 h followed by stimulation with αCD3 and αCD28. The resulting increase in cytokine production (as

Table 4. Optimization of Spiro-indolines

Cmpd	R ^a	cLogP	HPK1 K _i (nM) ^b	LLE ^c	LCK Selectivity ^d	Jurkat pSLP76 IC ₅₀ (μM) ^e	HLM ^f	MDCK P _{app} (x10 ⁶ cm/s) ^g	Cmpd	R ^a	cLogP	HPK1 K _i (nM) ^b	LLE ^c	LCK Selectivity ^d	Jurkat pSLP76 IC ₅₀ (μM) ^e	HLM ^f	MDCK P _{app} (x10 ⁶ cm/s) ^g
16		2.5	6.7	5.7	325x	1.5	17	23	23		1.1	63	6.1	267x	>25	4.7	0.8
17		1.5	8.4	6.6	482x	5.0	4.9	5.0	24		1.9	2.0	7.8	1722x	1.1	7.4	0.3
18		1.9	8.1	6.2	881x	2.0	9.5	4.1	25		1.9	0.8	8.2	2509x	0.44	6.9	0.3
19		2.3	8.2	5.8	316x	3.0	<3.9	5.7	26		1.9	85	6.2	179x	>25	6.1	0.4
20		2.2	11	6.2	414x	1.7	14	21	27		2.1	14	6.0	110x	15	9.9	0.4
21		2.6	8.4	5.5	98x	7.9	14	26	28		1.4	12 ^h	6.5	71x	1.7	18	7.1
22		0.75	1.8	8.0	2554x	1.3	7.4	0.2	29		1.8	1.1 ^h	7.2	1670x	1.2	19	6.5

^aRelative stereochemistry as drawn. Absolute stereochemistry as noted. ^bAll apparent K_i values represent arithmetic means of at least two determinations using the HPK1 Lantha binding biochemical assay. ^cLLE, lipophilic ligand efficiency based on HPK1 K_i. ^dSelectivity expressed as the ratio of LCK K_i over HPK1 K_i. ^eCellular assay that measures the direct phosphorylation of SLP76 by HPK1 in Jurkat cells. ^fHLM = Human liver microsome predicted clearance (mL/min/kg). ^gMDCK permeability assay (apical-to-basolateral). ^hApparent HPK1 K_i values for compounds 28 and 29 represent arithmetic means of two determinations using the HPK1 HTRF enzymatic assay.

measured by IL2 concentration) was then determined. As shown in Figure 3, treatment with 25 resulted in dose-dependent augmentation of IL2 production as one would

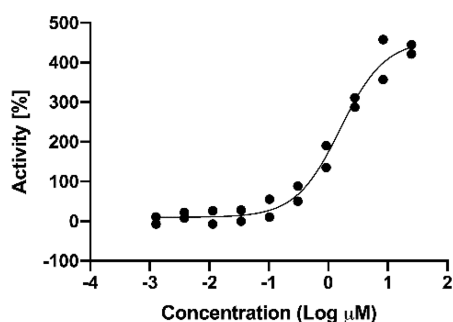


Figure 3. Dose–response curve measuring IL2 levels in human pan T-cell cultures after treatment with 25 followed by stimulation with αCD3 and αCD28 (calculated EC₅₀ = 1.56 ± 0.10 μM). Activity displayed as percent increase in IL2 concentration relative to stimulated/untreated controls. Data points represent results from two replicates.

expect from inhibition of HPK1 kinase activity. Further ADME-PK profiling showed that 25 addressed the two major liabilities of the original 7-azaindole HPK1 inhibitors: 25 demonstrated good metabolic stability in human hepatocytes (human hepatocyte clearance for 25 = 9.2 mL/min/kg; human hepatocyte clearance for 2 = 15 mL/min/kg) and minimal inhibitory activity against CYP3A4 (TDI IC₅₀ > 10 μM).

After an iv bolus dose in mouse, 25 showed a blood clearance of 57 mL/min/kg (Table 5). The good *in vitro*–*in vivo* correlation for mouse suggested that human liver microsomes and hepatocytes could be a reasonable predictor of metabolic stability in human. Despite its modest MDCK permeability, 25 showed 13% oral bioavailability in mouse after oral dosing using a suspension formulation (25 mg/kg; MCT suspension).

Herein, we described the lead optimization of a series of HPK1 inhibitors where improvement in selectivity was achieved by optimizing interactions with the induced, noncanonical P-loop conformation in HPK1. The key transformation in the lead optimization process to address metabolic liabilities included the conversion of the 7-azaindole to a series of spiroindoline motifs as the hinge-binding element. Results from optimization

Table 5. Pharmacokinetic Profile of 25

compd	LM H/R/M ^{a,d}	Hep H/R/M ^{b,d}	mouse iv CL, V _{ss} ^c	mouse F% ^c
25	6.9/8.7/38	9.5/18/33	57, 1.9	13%

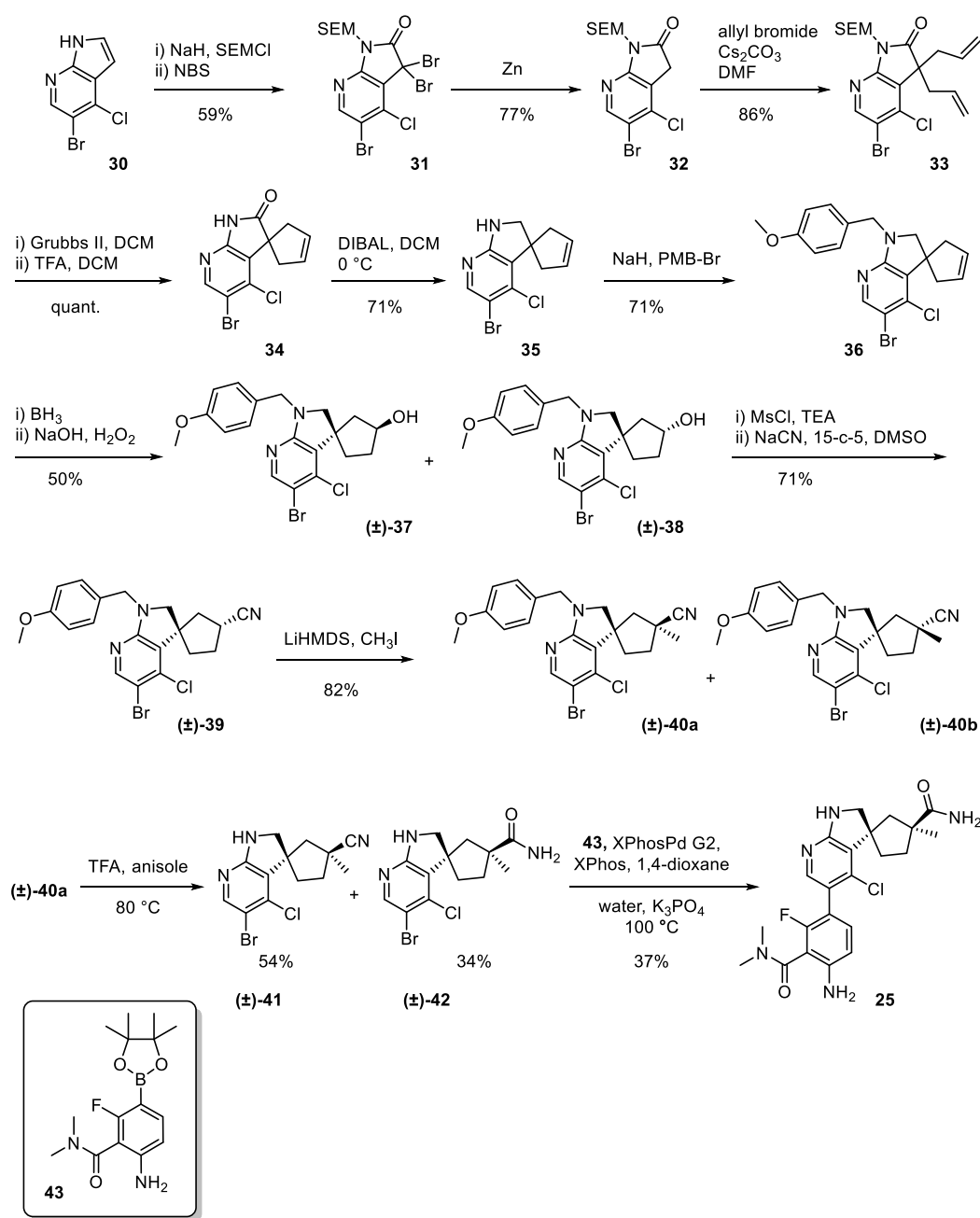
^aLM = Liver microsome predicted clearance (mL/min/kg), H = human, R = rat, M = mouse. ^bHep = Hepatocyte clearance measured in mL/min/kg, H = human, R = rat, M = mouse. ^cMouse PK: CS7BL/6, 1 mg/kg iv dose or 25 mg/kg po dose, blood clearance measured in mL/min/kg, V_{ss} = volume of distribution (L/kg). ^dHLM and Hep clearance values represent arithmetic means of two determinations.

of 25 to further improve its ADME properties will be disclosed in due course.

CHEMISTRY

As outlined in Scheme 1, the synthesis of 25 began with SEM protection of the commercially available 5-bromo-4-chloro-7-azaindole 30. The azaindole motif was then converted to the 3,3-dibromoxindole 31 via oxidative bromination with NBS. Zinc reduction then yielded oxindole 32. The spirocyclic cyclopentenyl ring was then installed via bis-alkylation using allyl bromide, followed by a ring-closing metathesis to give cyclopentene 34. The oxindole was then reduced and *N*-protected to give indoline 36. Hydroboration/oxidation then yielded a diastereomeric mixture of 37 and 38. The alcohol 37 was then advanced to the corresponding nitrile 39 by activating the alcohol via mesylation and cyanide displacement. α -Alkylation of the nitrile using methyl iodide then afforded a diastereomeric mixture of 40a and 40b (dr 4:1). Separation of the diastereomers was achieved via silica gel flash chromatography to yield 40a (racemic). Deprotection of the PMB group with concomitant hydrolysis using TFA yielded both the nitrile 41 and 42. Coupling of 41 with 43 using XPhosPd G2, XPhos, 1,4-dioxane, water, and K₃PO₄ at 100 °C yielded 25.

Scheme 1. Synthesis of Compound 25



41 (result of incomplete hydrolysis) and primary amide 42. Compound 42 was then coupled with the boronate 43¹⁵ to give (±)-25. The single enantiomers were separated using chiral supercritical fluid chromatography (SFC) to give 25 and 26. Other analogues described herein were prepared using a similar synthetic scheme. (Experimental procedures can be found in the [Supporting Information](#).)

■ ASSOCIATED CONTENT

SI Supporting Information

The Supporting Information is available free of charge at <https://pubs.acs.org/doi/10.1021/acsmmedchemlett.1c00473>.

Experimental procedures, compound characterization, detailed kinase selectivity panel data for compound 25, crystallographic statistics for protein cocrystal structures of 3, G1858, 14 and 17 ([PDF](#))

■ AUTHOR INFORMATION

Corresponding Author

Bryan K. Chan – Genentech Inc., South San Francisco, California 94080, United States; orcid.org/0000-0002-1086-4596; Email: chan.bryan@gene.com

Authors

Eileen Seward – Charles River Laboratories, Harlow, Essex CM19 5TR, United Kingdom
Michael Lainchbury – Charles River Laboratories, Harlow, Essex CM19 5TR, United Kingdom
Thomas F. Brewer – Genentech Inc., South San Francisco, California 94080, United States
Le An – Genentech Inc., South San Francisco, California 94080, United States
Toby Blench – Charles River Laboratories, Harlow, Essex CM19 5TR, United Kingdom; orcid.org/0000-0002-7401-9199
Matthew W. Cartwright – Charles River Laboratories, Harlow, Essex CM19 5TR, United Kingdom
Grace Ka Yan Chan – Genentech Inc., South San Francisco, California 94080, United States
Edna F. Choo – Genentech Inc., South San Francisco, California 94080, United States; orcid.org/0000-0003-4200-8302
Jason Drummond – Genentech Inc., South San Francisco, California 94080, United States
Richard L. Elliott – Charles River Laboratories, Harlow, Essex CM19 5TR, United Kingdom
Emanuela Gancia – Charles River Laboratories, Harlow, Essex CM19 5TR, United Kingdom
Lewis Gazzard – Genentech Inc., South San Francisco, California 94080, United States
Baihua Hu – Pharmaron Beijing Co, Beijing 100176, P.R. China
Graham E. Jones – Charles River Laboratories, Harlow, Essex CM19 5TR, United Kingdom
Xifeng Luo – Pharmaron Beijing Co, Beijing 100176, P.R. China
Andrew Madin – Charles River Laboratories, Harlow, Essex CM19 5TR, United Kingdom
Sushant Malhotra – Genentech Inc., South San Francisco, California 94080, United States
John G. Moffat – Genentech Inc., South San Francisco, California 94080, United States
Jodie Pang – Genentech Inc., South San Francisco, California 94080, United States

Laurent Salphati – Genentech Inc., South San Francisco, California 94080, United States
Christopher J. Sneeringer – Genentech Inc., South San Francisco, California 94080, United States
Craig E. Stivala – Genentech Inc., South San Francisco, California 94080, United States; orcid.org/0000-0002-5024-6346
Binqing Wei – Genentech Inc., South San Francisco, California 94080, United States
Weiru Wang – Genentech Inc., South San Francisco, California 94080, United States
Ping Wu – Genentech Inc., South San Francisco, California 94080, United States
Timothy P. Heffron – Genentech Inc., South San Francisco, California 94080, United States

Complete contact information is available at:

<https://pubs.acs.org/doi/10.1021/acsmmedchemlett.1c00473>

Notes

The authors declare no competing financial interest.

■ ACKNOWLEDGMENTS

We thank the Genentech Analytical Research, DMPK, in vivo Studies Group and Compound Management colleagues for their contributions. We also thank the Chemistry groups at Pharmaron, WuXi AppTec, and ChemPartner for their technical contributions. We thank the beamline staff at Advance Photon Source and Stanford Synchrotron Radiation Light-Source for their assistance in data collection.

■ ABBREVIATIONS

A, apical; Abl, Abl kinase; ADME, absorption, distribution, metabolism, elimination; B, basolateral; CL, clearance; CYP, cytochrome P450; F, oral bioavailability; Hep, hepatocytes; HLM, human liver microsomes; HPK1, Hematopoietic progenitor kinase 1; HTS, high-throughput screening; IL2, interleukin-2; iv, intravenous; LCK, lymphocyte-specific protein tyrosine kinase; LLE, ligand lipophilic efficiency; Liver Mic, liver microsomes assay; MCT, 0.5% methylcellulose with 0.2% Tween in water; MH, mouse hepatocytes; MLM, mouse liver microsomes; NBS, N-bromosuccinimide; P_{app}, apparent permeability; PK, pharmacokinetics; PMB, *para*-methoxybenzyl; po, oral administration; SEM, trimethylsilylethoxymethyl; SFC, supercritical fluid chromatography; SLP76, SH2-domain-containing leukocyte protein of 76 kDa; T, testosterone, TCR, T-cell receptor; TDI, time-dependent inhibition; TFA, trifluoroacetic acid; V_{ss}, volume of distribution at steady state

■ REFERENCES

- (1) (a) Chen, D. S.; Mellman, I. Oncology meets immunology: the cancer-immunity cycle. *Immunity* **2013**, *39*, 1–10. (b) Barbee, M. S.; Ogunniyi, A.; Horvat, T. Z.; Dang, T.-O. Current status and future directions of the immune checkpoint inhibitors ipilimumab, pembrolizumab, and nivolumab in oncology. *Ann. Pharmacother.* **2015**, *49*, 907–937. (c) Sharma, P.; Allison, J. P. Immune checkpoint targeting in cancer therapy: toward combination strategies with curative potential. *Cell* **2015**, *161*, 205–214.
- (2) (a) Mahoney, K. M.; Rennert, P. D.; Freeman, G. J. Combination cancer immunotherapy and new immunomodulatory targets. *Nat. Rev. Drug Discovery* **2015**, *14*, 561–584. (b) Heffron, T. P.; Chan, B. K. Small molecules for cancer immunotherapy. *Med. Chem. Rev.* **2017**, *52*, 219–241.

- (3) Sawasdikosol, S.; Zha, R.; Yang, B.; Burakoff, S. HPK1 as a novel target for cancer immunotherapy. *Immunol. Res.* **2012**, *54*, 262–265.
- (4) Hernandez, S.; Qing, J.; Thibodeau, R. H.; Du, X.; Park, S.; Lee, H.-M.; Xu, M.; Oh, S.; Navarro, A.; Roose-Girma, M.; Newman, R. J.; Warming, S.; Nannini, M.; Sampath, D.; Kim, J. M.; Grogan, J. L.; Mellman, I. The kinase activity of Hematopoietic Progenitor Kinase 1 is essential for the regulation of T cell function. *Cell Rep.* **2018**, *25*, 80–94.
- (5) (a) Sawasdikosol, S.; Burakoff, S. A perspective on HPK1 as a novel immuno-oncology drug target. *eLife* **2020**, *9*, No. e55122. (b) Degnan, A. P.; Kumi, G. K.; Allard, C. W.; Araujo, E. V.; Johnson, W. L.; Zimmermann, K.; Pearce, B. C.; Sheriff, S.; Futran, A.; Li, X.; Locke, G. A.; You, D.; Morrison, J.; Parrish, K. E.; Stromko, C.; Murtaza, A.; Liu, J.; Johnson, B. M.; Vite, G. D.; Wittman, M. D. Discovery of Orally Active Isofuranones as Potent, Selective Inhibitors of Hematopoietic Progenitor Kinase 1. *ACS Med. Chem. Lett.* **2021**, *12*, 443–450. (c) Yu, E. C.; Methot, J. L.; Fradera, X.; Lesburg, C. A.; Lacey, B. M.; Siliphaivanh, P.; Liu, P.; Smith, D. M.; Xu, Z.; Piesvaux, J. A.; Kawamura, S.; Xu, H.; Miller, J. R.; Bittinger, M.; Pasternak, A. Identification of Potent Reverse Indazole Inhibitors for HPK1. *ACS Med. Chem. Lett.* **2021**, *12*, 459–466. (d) Vara, B. A.; Levi, S. M.; Achab, A.; Candito, D. A.; Fradera, X.; Lesburg, C. A.; Kawamura, S.; Lacey, B. M.; Lim, J.; Methot, J. L.; Xu, Z.; Xu, H.; Smith, D. M.; Piesvaux, J. A.; Miller, J. R.; Bittinger, M.; Ranganath, S. H.; Bennett, D. J.; DiMauro, E. F.; Pasternak, A. Discovery of Diaminopyrimidine Carboxamide HPK1 inhibitors as Preclinical Immunotherapy Tool Compounds. *ACS Med. Chem. Lett.* **2021**, *12*, 653–661. (e) You, D.; Hillerman, S.; Locke, G.; Chaudhry, C.; Stromko, C.; Murtaza, A.; Fan, Y.; Koenitzer, J.; Chen, Y.; Briceno, S.; Bhadra, R.; Duperret, E.; Gullo-Brown, J.; Gao, C.; Zhao, D.; Feder, J.; Curtin, J.; Degnan, A. P.; Kumi, G.; Wittman, M.; Johnson, B. M.; Parrish, K. E.; Gokulrangan, G.; Morrison, J.; Quigley, M.; Hunt, J. T.; Salter-Cid, L.; Lees, E.; Sanjuan, M. A.; Liu, J. Enhanced antitumor immunity by a novel small molecule HPK1 inhibitor. *J. Immunother. Cancer* **2021**, *9*, No. e001402. (f) Linney, I. D.; Kaila, N. Inhibitors of immuno-oncology target HPK1 – a patent review (2016–2020). *Expert Opin. Ther. Pat.* **2021**, *31*, 893–910.
- (6) Arnold, W. D.; Bounaud, P.; Chen, C.; Eastman, B.; Gosberg, A.; Gradl, S. N.; Hopkins, S.; Li, Z.; McDonald, I.; Sprengeler, P. A.; Steensma, R. W.; Wilson, M. E. Preparation of pyrrolo[2,3-*b*]pyridine derivatives as kinase modulators. US patent 20090143352.
- (7) (a) Leeson, P. D.; Springthorpe, B. The influence of drug-like concepts on decision-making in medicinal chemistry. *Nat. Rev. Drug Discovery* **2007**, *6*, 881–890. (b) Hopkins, A. L.; Keserü, G. M.; Leeson, P. D.; Rees, D. C.; Reynolds, C. H. The role of ligand efficiency metrics in drug discovery. *Nat. Rev. Drug Discovery* **2014**, *13*, 105–121. (c) Ryckmans, T.; Edwards, M. P.; Horne, V. A.; Correia, A. M.; Owen, D. R.; Thompson, L. R.; Tran, I.; Tutt, M. F.; Young, T. Rapid assessment of a novel series of selective CB₂ agonists using parallel synthesis protocols: A Lipophilic Efficiency (LipE) analysis. *Bioorg. Med. Chem. Lett.* **2009**, *19*, 4406–4409.
- (8) Wang, J. Y. J. The capable ABL: what is its biological function? *Mol. Cell. Biol.* **2014**, *34*, 1188–1197.
- (9) Palacios, E. H.; Weiss, A. Function of the Src-family kinases, Lck and Fyn, in T-cell development and activation. *Oncogene* **2004**, *23*, 7990–8000.
- (10) Hantschel, O. Structure, regulation, signaling, and targeting of abl kinases in cancer. *Genes Cancer* **2012**, *3*, 436–446.
- (11) Guimarães, C. R.; Rai, B. K.; Munchhof, M. J.; Liu, S.; Wang, J.; Bhattacharya, S. K.; Buckbinder, L. Understanding the impact of the P-loop conformation on kinase selectivity. *J. Chem. Inf. Model.* **2011**, *51*, 1199–1204.
- (12) Wu, P.; Sneider, C. J.; Pitts, K. E.; Day, E. S.; Chan, B. K.; Wei, B.; Lehoux, I.; Mortara, K.; Li, H.; Wu, J.; Franke, Y.; Moffat, J. G.; Grogan, J. L.; Heffron, T. P.; Wang, W. Hematopoietic Progenitor Kinase-1 structure in a domain-swapped dimer. *Structure* **2019**, *27*, 125–133.
- (13) Collie, G. W.; Michaelides, I. N.; Embrey, K.; Stubbs, C. J.; Börjesson, U.; Dale, I. L.; Snijder, A.; Barlind, L.; Song, K.; Khurana, P.; Phillips, C.; Storer, R. I. Structural Basis for Targeting the Folded P-Loop Conformation of c-MET. *ACS Med. Chem. Lett.* **2021**, *12*, 162–167.
- (14) Johnson, M. G.; Liu, J. J.; Li, A.-R.; van Lengerich, B.; Wang, S.; Medina, J. C.; Collins, T. L.; Danao, J.; Seitz, L.; Willee, A.; D'Souza, W.; Budelsky, A. L.; Fan, P. W.; Wong, S. G. W. Solving time-dependent CYP3A4 inhibition for a series of indole-phenylacetic acid dual antagonists of the PGD₂ receptors CRTH2 and DP. *Bioorg. Med. Chem. Lett.* **2014**, *24*, 2877–2880.
- (15) Synthesis of compound **43** is described in the [Supporting Information](#).